Synthesis and characterization of a biocompatible nanoplatform based on silica-embedded SPIONs functionalized with polydopamine

Journal:	*ACS Biomaterials Science & Engineering*
Manuscript ID	ab-2022-00946x
Manuscript Type:	Article
Date Submitted by the Author:	11-Aug-2022
Complete List of Authors:	Romano, Miriam; Università degli Studi di Brescia; Center for Colloid and Surface Science; Helmholtz Center Munich German Research Center for Environmental Health González Gómez, Manuel; Universidade de Santiago de Compostela, Applied Physics Department Santonicola, Pamela; IBBR CNR Aloi, Noemi; Institute for Biomedical Research and Innovation National Research Council Offer, Svenja; Helmholtz Center Munich German Research Center for Environmental Health; University of Rostock Pantzke, Jana; Helmholtz Center Munich German Research Center for Environmental Health; University of Rostock Raccosta, Samuele; National Research Council of Italy, Institute of Biophysics Longo, Valeria; Institute for Biomedical Research and Innovation National Research Council Surpi, Alessandro; Institute of Nanostructured Materials Support Unit of Bologna Zampi, Giuseppina; IBBR CNR Dediu, Valentin; Institute of Nanostructured Materials Support Unit of Bologna Zimmermann, Ralf; Helmholtz Center Munich German Research Center for Environmental Health; University of Rostock Manno, Mauro; National Research Council of Italy, Institute of Biophysics Piñeiro, Yolanda; Universidade de Santiago de Compostela, Fisica Aplicada Facultade de Física Colombo, Paolo; Institute for Biomedical Research and Innovation National Research Council Schiavi, Elia Di; IBBR CNR, Rivas, Jose; Universidade de Santiago de Compostela, Fisica Aplicada Facultade de Física BERGESE, Paolo; Universita degli Studi di Brescia, Department of Molecular and Translational Medicine and INSTM; Center for Colloid and Surface Science Di Bucchianico, Sebastiano; Helmholtz Center Munich German Research Center for Environmental Health, Comprehensive Molecular Analytics

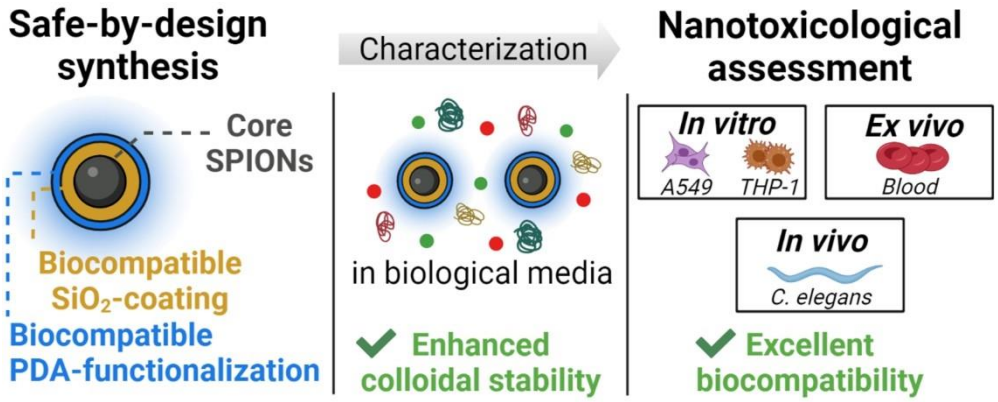

Table of Content (TOC) graphics

151x60mm (300 x 300 DPI)

Synthesis and characterization of a biocompatible nanoplatform based on silica-embedded SPIONs functionalized with polydopamine

*Miriam Romano[1,2,3], Manuel Antonio González Gómez[4], Pamela Santonicola[5], Noemi Aloi[6], Svenja Offer[3], Jana Pantzke[3], Samuele Raccosta[7], Valeria Longo[6], Alessandro Surpi[8], Giuseppina Zampi[5], Valentin Alek Dediu[8], Ralf Zimmerman[3], Mauro Manno[7], Yolanda Piñeiro[4], Paolo Colombo[6], Elia Di Schiavi[5], José Rivas[4], Paolo Bergese[1,2], Sebastiano Di Bucchianico[3]**

[1] Department of Molecular and Translational Medicine, University of Brescia, Brescia, Italy

[2] Center for Colloid and Surface Science (CSGI), Florence, Italy

[3] Joint Mass Spectrometry Center (JMSC) at Comprehensive Molecular Analytics, Helmholtz Zentrum München, Neuherberg, Germany

[4] NANOMAG Laboratory, Applied Physics Department, iMATUS Materials Institute, Universidade de Santiago de Compostela, Santiago de Compostela, Spain

[5] Institute of Biosciences and BioResources (IBBR), National Research Council of Italy (CNR), Naples, Italy

[6] Institute for Biomedical Research and Innovation (IRIB), National Research Council of Italy (CNR), Palermo, Italy

[7] Institute of Biophysics (IBF), National Research Council of Italy (CNR), Palermo, Italy

[8] Institute of Nanostructured Materials (ISMN), National Research Council of Italy (CNR), Bologna, Italy

*corresponding author: dibucchianico@helmholtz-muenchen.de

Abstract

Superparamagnetic Iron Oxide Nanoparticles (SPIONs) have gained increasing interest in nanomedicine, but most of those reached the clinical trials have been withdrawn due to toxicity concerns. Therefore, there is an urgent need to design low-risk and biocompatible SPION formulations. In this work, we present an original safe-by-design nanoplatform made of silica nanoparticles loaded with SPIONs and decorated with polydopamine (SPIONs@SiO2-PDA) and the study of its biocompatibility performances by an ad-hoc thorough in vitro to in vivo nanotoxicological methodology. The results indicate that the SPIONs@SiO2-PDA have excellent colloidal stability in serum-supplemented culture media, even after long-term (24h) exposures, showing no cytotoxic or genotoxic effects in vitro and ex vivo. Physiological responses, evaluated in vivo using Caenorhabditis elegans as animal model, showed no impact on fertility and embryonic viability, induction of oxidative stress response, and a mild impact on animal locomotion. These tests indicate that the synergistic combination of silica matrix and PDA coating we developed effectively protects the SPIONs, providing enhanced colloidal stability and excellent biocompatibility.

KEYWORDS

SPION; silica; coating materials; polydopamine; nanotoxicity; *C. elegans*

Introduction

Superparamagnetic Iron Oxide Nanoparticles (SPIONs) are among the most investigated magnetic nanoparticles (MNPs) due to their high responsivity to magnetic fields. Namely, SPIONs possess null magnetic remanence combined with high saturation magnetization that assures no inter-particle magnetic interactions in the absence of external magnetic fields and a fast and robust response when the latter is applied [1]. This characteristic fundamentally opens up broad horizons for their use in guided and controllable nanoparticle (NP) targeting and activity under magnetic fields. Being easily manageable by using external fields, SPIONs have gained interest in a wide range of applications, from magnetic resonance imaging (MRI) [2] to cell/tissue targeting or magnetic hyperthermia

treatments (MHT) [3]. SPIONs' architecture is mainly based on maghemite (γ-Fe_2O_3) or magnetite (Fe_3O_4) cores covered by an external coating [4] which steers NP interactions within the biological environment. SPION surface coatings provide augmented colloidal stability [5], and several efforts have been attempted to design and synthesize clinical-ready low-risk SPIONs coated with biocompatible shells mostly made of dextran or dextran-derivatives (e.g., Endorem® or Resovist®) [6,7]. In general, the nature of the surface shells (along with the size) represents a key factor in determining SPION uptake, toxicity [8], and biodistribution profiles [4,9,10]. In this regard, silica (SiO_2) and bioinspired polydopamine (PDA) coatings can endow SPIONs with interesting biological and optical properties. From a biological standpoint, it has already been demonstrated that silica shells can lessen SPION cytotoxic effects by preventing corrosion and inhibiting iron ion release [11]. On the other hand, PDA emerged as promising NP coating material due to its natural origin [12]. Furthermore, PDA is highly reactive and can be used to increase NPs' drug binding/loading processes and release efficiencies [13], feasible for drug delivery in targeted therapies. Both silica-embedded and PDA-functionalized SPIONs have already been applied in several *in vitro* and *in vivo* pre-clinical studies for their use as drug delivery systems [14,15], MHT [16], and MRI agents [17,18]. Furthermore, PDA manifests UVA-induced fluorescence [19], which can provide silica-coated SPIONs with distinct optical properties exploitable for *in vitro* or *ex vivo* fluorescent analysis.

PDA coating is usually made through PDA-self polymerization by immersing NPs in a PDA alkaline aqueous solution [12]. Despite being considered a gold-standard method, several parameters like temperature and pH can affect the coating efficiency of this process [13,20], leading to high-grade batch-to-batch variability. Furthermore, chemical residues from Tris hydrochloride – commonly used to create an alkaline environment [13]– can contribute to unexpected toxic side effects. In this case, a different safe-by-design approach can help reduce risks, safeguarding SPIONs' synthetic reproducibility. Here, we present a novel nanoplatform made of silica nanoparticles loaded with SPIONs and functionalized with polydopamine (SPIONs@SiO_2-PDA) by a biocompatible, highly reproducible, and cost-effective procedure. We also provide an extensive, stepwise biological and

nanotoxicological characterization *in vitro, ex vivo,* and *in vivo* as required in the Minimum Information reporting in bio-nano experimental literature (MIRIBEL)[21]. SPIONs@SiO_2-PDA biocompatibility was assessed by a broad set of toxicological assays *in vitro,* in A549 cancerous alveolar epithelial lung cell line, and in monocyte/macrophage THP-1 cells, *ex vivo* in whole human blood, and *in vivo* using *C. elegans* as animal model. Throughout all the three biological characterization steps, we observed no cytotoxicity or genotoxicity and mild effects *in vivo* on animal locomotion. Responsiveness to external magnetic fields and SPIONs@SiO_2-PDA capability to be effectively concentrated in sub-millimeters sized regions by external magnets confirmed their potential for future theranostic applications.

Materials and methods

Synthesis of silica-embedded SPIONs functionalized with polydopamine (SPIONs@SiO_2-PDA)

SPIONs@SiO_2-PDA were obtained using three synthetic steps, including co-precipitation, microemulsion, and polymerization (Fig.1a). Step 1 led to the production of iron oxide NPs coated with oleic acid (SPIONs@OA) by co-precipitation, according to the reaction equation:

$$Fe^{2+} + 2Fe^{3+} + 8OH^- \rightarrow Fe_3O_4 + 4H_2O \rightarrow 2Fe(OH)_3 \; Fe(OH)_2 \rightarrow Fe_3O_4 + 4H_2O$$

Keeping the molar ratio 1:2 for total precipitation of Fe_3O_4 in a reducing environment, as described in González-Gómez *et al.* [22], with some modifications related to the washing procedure of the obtained hydrophobic MNPs (S1). In step 2, SPIONs@OA were coated with silica (SPIONs@SiO_2) by a water-in-cyclohexane reverse microemulsion process, as reported by Moldes *et al.*[23]. Experimental details can be found in S1. SPIONs@SiO_2 were washed four times using 2-propanol (IPA, C_3H_8O). SPIONs@SiO_2 were retained with a permanent magnet for each wash, and the supernatant was removed. SPIONs@SiO_2 were washed twice with Milli-Q water, centrifuged at 9000 rpm for 15 min, and redispersed in Milli-Q water. Finally, step 3 led to the functionalization of SPIONs@SiO_2 with polydopamine (SPIONs@SiO_2-PDA) based on the dopamine polymerization on SPIONs@SiO_2. Firstly, SPIONs@SiO_2 (31 mg) were dispersed in 10 mL of Milli-Q water. Then

NH_4OH (1 mmol) and dopamine hydrochloride (DA, $C_8H_{11}NO_2 \cdot HCl$, 0.19 mmol) were added and incubated at 70°C overnight. SPIONs@SiO_2-PDA were separated from the reaction medium by a magnetic field and washed six times with Milli-Q water. Finally, SPIONs@SiO_2-PDA were re-dispersed in Milli-Q water to a final concentration of 0.1 % wt (256 μg) determined by thermogravimetric analysis (TGA) and flame atomic absorption spectroscopy (FAAS). All solvents and chemicals were analytical grade and purchased from Sigma-Aldrich.

Physicochemical, optical and magnetic characterization of SPIONs@SiO_2-PDA

X-ray diffraction was performed with an X-ray diffractometer using a Philips PW1710 diffractometer (Panalytical) operated at 40 kV and 30 mA, and the spectrum was recorded by Cu-Kα radiation source (λ= 1.54186 Å). Measurements were collected in the 2Θ angle range between 10° and 80° with steps of 0.02° and 10 s/step. Surface functional groups of dried SPIONs were analyzed by Fourier Transform Infrared (FTIR) Spectroscopy with a Thermo Nicolet Nexus spectrometer (Thermo Fisher Scientific) using the attenuated total reflectance (ATR) method from 4000 to 400 cm^{-1}. The morphology and size were studied by transmission electron microscopy (TEM) using a JEOL JEM-1011 microscope operating at 100 kV. Samples were placed on copper grids with Formvar® films for analysis, and the diameter was measured using ImageJ software. Iron content in the MNPs samples was determined by FAAS performed with an Atomic Absorption Spectrometer (Perkin Elmer 3110, Perkin). The composition of the samples was analyzed with a TGA Perkin Elmer model 8000 (Perkin). SPIONs@SiO_2-PDA fluorescence was acquired with a Leica TCS SP8 SMD confocal microscope with an HC PL APO CS 63×1.40 OIL objective with a 54.4% 405 nm laser (1024×1024-pixel images, bidirectional scan direction). SPIONs@SiO_2-PDA magnetic properties were measured by using a vibrating sample magnetometer (VSM) (DMS/ADE Technologies) and a superconducting quantum interference device (SQUID) magnetometer (Quantum Design, model MPMS-5). Magnetization data were normalized to the magnetic mass (Wmag) amount for each sample (determined by TGA). A microscope-connected CCD camera (Dino-Lite Pro, AnMo Electronics Corporation, Hsinchu City, Taiwan) has been used to follow the behavior of SPION solutions

contained inside 500 µm wide quartz capillaries (WJM-Glass/Müller GmbH, Berlin, Germany) under the influence of the magnetic field. A 0.9 mm wide tubing in medical-grade silicon (Silastic® Rx 50 medical grade tubing, Dow Corning, Midland, Michigan (USA) connected to a peristaltic pump (120s, Watson Marlow, Cheltenham, UK) feds the capillary with nanoparticle solutions.

Cell culture

A549 cells (ATCC; CCL-185) were cultured in high-glucose Dulbecco's Modified Eagle Medium: Nutrient Mixture F-12 (DMEM:F-12) (ThermoFisher Scientific, 31331-028) supplemented with 5% (vol/vol) fetal bovine serum (FBS) (ThermoFisher Scientific, 10500-064) and 100 U/mL penicillin and 100 µg/mL streptomycin (P/S; Sigma-Aldrich, P4333) hereafter referred to as completeDMEM:F12 media (cDMEM:F12) . The human monocytic leukemia THP-1 cell line (ECACC 88081201) was maintained in culture with RPMI 1640 medium (Gibco, Life Technologies, 52400-025) supplemented with heat-inactivated 10% FBS (Gibco, Life Technologies, 10270-106) and 1% P/S (Gibco, Life Technologies, 15070-063), hereafter referred to as completeRPMI (cRPMI). Differentiated THP-1 monocytes with a macrophage-like phenotype M0 (THP-1 M0) were obtained by treating cells with 200 nM phorbol 12-myristate-13-acetate (PMA; Sigma, P8139) for 72 hours. A549 and THP-1 cells were maintained in a humidified incubator at 37°C in 5% carbon dioxide (CO_2).

Dynamic light scattering measurements in culture media

SPIONs@SiO_2-PDA fresh aliquot (1mg/mL) was vortexed for 3 minutes and then centrifuged at 4 °C for 10 minutes at 1000 g. 50 µg/mL SPIONs@SiO_2-PDA dispersions were prepared in the following buffers: (i) milliQ H_2O, (ii) RPMI + 1% P/S [RPMI], (iii) cRPMI, (iv) DMEM:F12+ 1% P/S [DMEM:F12], (v) cDMEM:F12. Samples were put into quartz cuvettes and incubated at 37 °C for 0h, 4h, and 24h. The cells were transferred in a cell compartment of a BI200-SM goniometer (Brookhaven Instruments), thermostated at 20 °C, and equipped with a He-Ne laser (JDS Uniphase 1136P) with wavelength λ = 633 nm and a single-pixel photon counting module (Hamamatsu C11202-050). Scattered light intensity and its autocorrelation function $g_2(t)$ were measured

simultaneously at a scattering angle θ = 90° using a BI-9000 correlator (Brookhaven Instruments). The electric field autocorrelation function $g_1(t)$ was calculated by using the Siegert relation

$$g_2(t) = 1 + \beta |g_1(t)|^2 \quad (1)$$

where β is an instrumental parameter [24] and $g_1(t)$ is the field autocorrelation function, associated with the size (σ) of diffusing particles and their size distribution ($P_q(\sigma)$) by the relation

$$g_1(t) = \int P_q(\sigma) \exp\{-D(\sigma)q^2t\}\, d\sigma \quad (2)$$

where $q = 4\pi\tilde{n}\lambda^{-1}\sin(\theta/2)$ is the scattering vector in a medium with ñ refractive index and D(σ) is the diffusion coefficient of a particle of hydrodynamic diameter $D_h = \sigma$, determined by the Stokes-Einstein relation $D(\sigma) = kBT[3\pi\eta\sigma]^{-1}$, with T being the temperature, η the medium viscosity and k_B the Boltzmann constant. The refractive indexes (ñ) of each medium were measured by using an Abbe refractometer and taken as (i) 1.3320, (ii) 1.3346, (iii) 1.3350, (iv) 1.3347, (v) 1.3355. The medium viscosities (η) were calculated by interpolating the value reported in ref. [25] and taken as (i) 1.002, (ii) 1.111, (iii) 1.311, (iv) 1.115, (v) 1.457. The size distribution $P_q(\sigma)$ was calculated by assuming that the diffusion coefficient distribution was shaped as a Schultz distribution, which is a two-parameter asymmetric distribution, determined by the average diffusion coefficient <D> and its variance V [26,27]. Two robust parameters derived from this analysis: D_z, the z-averaged hydrodynamic diameter (the diameter corresponding to the average diffusion coefficient <D>), and PDI, the polydispersity index (here calculated as $PDI = V <D>^{-2}$), an estimation of the distribution width. The buffers containing FBS displayed a non-null intensity autocorrelation function due to the presence of several NPs. In this case, the field autocorrelation function of the medium $g_1^M(t)$ was measured, and then the NP autocorrelation function $g_1^{NP}(t)$ was calculated by a forced fit fixing the medium component:

$$|g_1(t)|^2 = | \alpha\, g_1^M(t) + (1-\alpha)\, g_1^{NP}(t) |^2 \quad (3)$$

where α = 0.95 is the fraction of integer medium in the sample [28,29].

Preparation of SPIONs@SiO_2-PDA dispersions in culture media and cell treatments

For A549 cell treatments, SPIONs@SiO_2-PDA solutions (1 mg/mL) were vortexed for 3 minutes at the highest speed using the Advanced IR Vortex Mixer Zx4 (VELP®scientifica) and diluted 1:10 in DMEM:F12 with GlutaMAX™, with or without 5% FBS. The 1:10 dilution was sonicated for 1 min with the Pals sonic ultrasonic cleaner (ALLPAX Germany) and finally, the suspensions were diluted to final concentrations and immediately used for cell exposures. For THP-1 cell treatments, SPIONs@SiO_2-PDA solutions (1 mg/mL) were vortexed and resuspended as described above in cRPMI 1640 medium and immediately used for cell treatment. A549 and THP-1 M0 cell treatments were carried out in 24-well (Corning, 3524) and 96-well (Corning, 3598) tissue culture plates, respectively, and cells were exposed to SPIONs@SiO_2-PDA dispersions in four different concentrations ranging from 0.1 µg/mL up to 50 µg/mL (corresponding to a range of 0.3 µg/cm^2 – 13.16 µg/cm^2 for A549 and 1.8 µg/cm^2 – 78.96 µg/cm^2 for THP-1 M0). For A549 exposures, cells were seeded as 3.5 x 10^4 cells/cm^2 in cDMEM: F12 media and treated for 4h or 24h in DMEM:F12 media (supplemented with 1% P/S) with or without 5 % serum. For THP-1 M0 exposures, cells were seeded as 1.0 x 10^5 cells/cm^2 in cRPMI media and treated for 24h, 48h, and 72h in cRPMI media.

Endotoxin assessment

Since endotoxins may interfere with the functional immunoassays, the potential presence of endotoxins in the sample preparations was assessed using the Multi-test Limulus Amebocyte Lysate (LAL) pyrogen plus test (Lonza, N594-03) (Gel Cloth LAL assay endogenous endotoxin content ≤ 0.003 EU/mL). Serial two-fold dilutions of each sample were tested until an endpoint was reached. SPIONs@SiO_2-PDA were compared to an internal standard control corresponding to decreasing endotoxin concentrations with positive (high concentration of endotoxin) and negative control (H_2O LAL as pyrogen-free water). The lysate sensitivity was calculated by determining the geometric mean of the endpoint. Each endpoint value was converted to log10. The individual log10 values were averaged, and the lysate sensitivity was taken as the antilog10 of this average log value.

Alamar blue assay

Alamar Blue assay was used to evaluate the metabolic activity of A549 cells. The exposure medium was removed, and A549 cells were washed once with DPBS 1X without $CaCl_2$ and $MgCl_2$ (Gibco, 14190-094) before adding 500 µl of pre-warmed fresh exposure media (DMEM: F12 + 1 % P/S with or without 5 % FBS) containing 10% PrestoBlue™ HS Cell Viability Reagent (ThermoFisher Scientific, A13262). After an incubation of 1 h at 37°C in 5% CO_2, the fluorescence (Ex 565nm; Em 590nm) was measured using the Varioskan LUX plate reader equipped with SkanIt Software 4.1 for Microplate Readers RE, ver. 4.1.0.43 (MULTISKAN SKY Microplate Spectrophotometer, ThermoFisher Scientific). Background fluorescence (PrestoBlue solutions in medium with or without serum) was subtracted from each well, and data were normalized to the control cells. Data from three independent experiments are expressed as mean ± standard error mean (SEM).

Lactate dehydrogenase assay

The Lactate Dehydrogenase (LDH) assay was used to assess the cytotoxicity in A549 cells by measuring the LDH leakage into the cell culture media upon plasma membrane disruption. After the exposure, supernatants from each well were collected, and the assay was carried out using the LDH activity kit (Roche, S-11644793001) with 100 µL of the supernatant following the supplier's instructions. Untreated cells incubated for 20 minutes with 0.2 % Triton-X (Sigma-Aldrich, 9036-19-5) were used as positive controls (PC). Absorbance at 490 nm and 630 nm were recorded with a Varioskan LUX plate reader provided with SkanIt Software 4.1 for Microplate Readers RE, ver. 4.1.0.43 (ThermoFisher Scientific). The absorbance values of the background controls (medium with or without serum) were removed from each sample. The results from three independent experiments are expressed as LDH (%) = [(average of treated cell values - lowest control value)/ (average of positive control – lowest control value) × 100] and the corresponding SEM. The lowest control value corresponds to spontaneous LDH activity, while the positive control represents the maximum.

Colony Forming Efficiency assay

The Colony Forming Efficiency (CFE) assay was applied to measure the clonogenicity of A549 cells upon treatment. The exposure medium was removed, and cells were washed once with DPBS. Cells were trypsinized with 0.05 % trypsin-EDTA solution (Sigma-Aldrich, T4174) for 1 minute at RT, and the trypsin-EDTA solution was removed, and the cells were incubated for further 3 minutes at 37°C. Cells were then resuspended in 500 µL of 5 % FBS DMEM: F12 media and centrifuged for 7 minutes at 200 g with a Heraeus Fresco17 microcentrifuge (ThermoFisher Scientific) at 4°C. The supernatant was discharged, and cells were resuspended in 300 µL of complete media (5% FBS). Cells were diluted 1:1 with Trypan Blue (logosbio, T13001) and counted with a Neubauer chamber (Marienfeld). Cells were finally seeded as 300 cells/well in 6-well plates in duplicates for each treatment. The medium was changed every two days. After ten days, cells were fixed with 3.5% (v/v) of formaldehyde solution (Carl Roth, 4980.1) in DPBS 1× without $CaCl_2$ and $MgCl_2$ and stained with 10% (v/v) Giemsa solution (PanReac AppliChem, 251337) in MilliQ water. Colonies composed of at least 50 cells were counted with Fiji software [30]. The results from three independent experiments are expressed as CFE (%) = [(average number of treatment colonies/average number of control colonies) × 100] and the corresponding SEM (n=3).

Genotoxicity

Single- and double-strand DNA breaks were assessed using the alkaline mini-gel COMET assay described in Di Bucchianico et al. [31]. Briefly, A549 cells were harvested, and 20 µl of cell suspension (250000 cells/mL) were mixed with 140 µl of 1% low gelling temperature agarose (Sigma–Aldrich, A9414) at 37°C. 20 µl aliquots were loaded as drops onto microscopy slides coated with 0.5% standard gelling temperature agarose (Sigma-Aldrich, 05066). Mini-gels underwent 1 h of lysis, followed by 40 min of alkaline treatment and subsequent electrophoretic separation for 25 min (270–300 mA, 1.2 V/cm^2). Slides were neutralized by washing twice with 0.4 M TRIS (Carl Roth, A411.1) and once with ultrapure water. The slides were air-dried at least overnight, and DNA was stained with SYBR GOLD (Invitrogen, S7563) in a 1:10000 dilution. Pictures were taken with a fluorescence microscope (20× magnification, BioTek Lionheart FX), and CometScore 2.0 software (TriTek Corp)

was used to manually score 50 nucleoids per mini-gel. Two mini-gels per sample were prepared, and three independent exposures were performed. Results were expressed as mean % DNA in tail ± SEM (n = 3). Cells treated with 30 μM hydrogen peroxide (H_2O_2, Merck, Darmstadt, Germany, 107209) for 5 min on ice were used as a positive control.

Malondialdehyde quantification

Malondialdehyde (MDA) content, an end product of lipid peroxidation, was measured to investigate oxidative stress. After the exposure, 80 μL of each well's supernatant was collected and frozen at -80°C. Samples were analyzed by LC-MS/MS according to an already published method without modifications [32]. MDA contents (ng/mL) were normalized with the Metabolic Cell Equivalents (MCE) [33] derived from the LDH data of the corresponding treatment wells and expressed as the mean of two independent experiments, each with two technical replicates, ± SEM (n=2).

MTS Assay

THP-1 cell viability was determined in vitro by 3-(4,5-dimethylthiazol-2-yl)-5-(3-carboxymethoxyphenyl)-2-(4-sulfophenyl)-2H-tetrazolium) MTS assay, using the CellTiter 96® Aqueous One Solution Cell Proliferation Assay kit (Promega, G3582) according to the manufacturer's protocol. After the exposure, 20 μl of MTS solution were added, and the cells were further incubated under the same conditions for an additional 2 h. The absorbance of the dissolved formazan was measured with an automated microplate reader (Imark Plate Reader, BioRad) at 490 nm. Cell viability percentage was determined as the ratio between the absorbance (OD) of treated and control cells x 100. Control cells were defined as cells treated with the medium only.

Hemolysis assay

Heparinized blood samples were obtained from three healthy human subjects. SPIONs@SiO_2-PDA were added to an 8% human erythrocytes solution and incubated at 37 °C for 30 min. The samples were centrifuged at 2000 x g for 5 min, and the supernatant absorbance was measured at 415 nm through the iMark™ Microplate Absorbance Reader (BioRad, Hercules) to determine the percentage of hemolysis. Triton X-100 1% solution and 1X PBS were taken as 100% and 0% of hemoglobin

release, respectively. Haemolysis percentage was determined as the ratio between the OD of treated cells and positive control cells.

Flow cytometry-based basophil activation test

Heparinized peripheral blood was obtained from 4 volunteers, and SPIONs@SiO_2-PDA potential allergenic activity was studied by basophil activation in whole blood samples by flow cytometry detecting the combination of the CCR3 and CD63 markers. Blood aliquots (100 µl) were incubated with SPIONs@SiO_2-PDA dilutions in cRPMI for 15 minutes at 37°C. PBS and anti-FcEpsilonRI were used as negative and positive controls, respectively. Basophils were detected, as previously reported in Bonura et al. [34]. The study was approved by the local Ethics Committee (Comitato Etico Palermo 1, 24 February 2021, resolution n. 02/2021).

Confocal microscopy

A549 cells were seeded on 12 mm-sized coverslips as 45000 cells in 150 µL of complete media. After 24 h, cells were exposed to 50 µg/mL (corresponding to 13,16 µg/cm^2) in media with or without 5% serum for 4 h and 24 h. The culture media was removed at each endpoint, cells were washed with DPBS without $CaCl_2$ and $MgCl_2$ and then fixed with 3.5 % formaldehyde solution for 15 minutes at RT. Cells were washed twice with 0.05 % Tween-20 (Chem Cruz, K0316) in DPBS (washing buffer) and permeabilized with 0.2 % Triton X-100 (Sigma Aldrich, 7BJ3924) in DPBS for 15 minutes at RT. After two other washing steps in DPBS unspecific binding was blocked with 1 % BSA and 0.1 % Triton-X 100 (blocking buffer) in DPBS for 30 min at RT. The cytoskeleton was stained with Alexa594 phalloidin (1:40 in blocking buffer; ThermoFisher Scientific, A12381) for 1 h at RT. Slides were washed three times with washing buffer and further incubated with NucGreen™ Dead 488 (3 drops in 1.5 ml H_2O; Invitrogen, R37109) for 15 min. Coverslips were washed three times with the washing buffer and then embedded by using mounting medium (Glycergel, DAKO, Agilent, C056330-2). 1636 x 1636 pixel images were acquired with a Zeiss LSM880 with a C-Apochromat 63x/1.20 W Korr M27 objective.

Assays *in vivo* in *C. elegans*

Nematodes have been grown and handled following standard procedures under uncrowded conditions on nematode growth medium (NGM) agar plates seeded with *Escherichia coli* strain OP50 [35]. Strains used in this work have been provided by the *Caenorhabditis* Genetics Center (CGC), which is funded by NIH Office of Research Infrastructure Programs (P40 OD010440): wild-type strain N2, Bristol variety; CL2166 *dvIs19* [(pAF15) *pgst-4*::GFP::NLS] that expresses an oxidative stress-responsive GFP. Animal treatments with SPIONs@SiO_2-PDA and Milli-Q water as mock were performed *in liquido* in 96-multiwell plates for the entire life-cycle of the animals (chronic treatment) [36]. Synchronized eggs, obtained by bleaching, were resuspended in M9 buffer (3 g KH_2PO_4; 6 g Na_2HPO_4; 5 g NaCl; 1 M $MgSO_4$; H_2O to 1 litre) with 2x antibiotic/antimycotic solution (Sigma-Aldrich, A5955), 5 ng/ml cholesterol and OP50. 60µL containing ~30 eggs were aliquoted in each well. SPIONs@SiO_2-PDA solutions were prepared for animal treatment as described before, diluted in Milli-Q water and added to the solution containing the animals at the final concentrations of 0.01, 0.1, 1, 10, and 50 µg/mL for thrashing assay, and 50 µg/mL for brood size, embryonic lethality, SWIP, and *pgst-4::*GFP expression. To evaluate SPIONs@SiO_2-PDA effects on brood size and embryonic lethality, 20 hermaphrodite animals at L4 stage treated as described above were transferred to new plates every 24 hours for all the fertile period of the animals (4 days) and the number of laid and hatched eggs were counted every day. Treatments were performed twice and in triplicate. To test SPIONs@SiO_2-PDA effect on animal movement, a thrashing assay was performed on young adult hermaphrodite animals transferred in 7µL of M9 buffer. Animals were left 5 minutes in buffer and then video recorded for 30 seconds. The measurement of thrashing was done counting every change of direction respect to the longitudinal axis of the body. Treatments were performed twice and in triplicate. SWimming-Induced Paralysis (SWIP) assay was performed to test a putative effect of polydopamine on animal motility [37]. Hermaphrodite animals were cleaned from bacteria by allowing them to crawl on an empty plate for 5 minutes before each experiment. 10 young adult hermaphrodite animals were placed into 40µL of M9 buffer in a watch glass, and their paralysis was scored after 10 minutes. Treatments were performed in triplicate. *pgst-4::*GFP expression was quantified after

treatment when hermaphrodite animals reached the young adult stage. 5 animals were transferred on each glass slide with 4% agar pad and immobilized alive for microscopy analysis with 100mM NaN_3 (Sigma-Aldrich, S8032) [38]. Epi-fluorescence images were collected with a Leica TCS SP8 AOBS inverted microscope, using a 10x objective and FITC filter. Fluorescence quantification was performed using ImageJ, and the Corrected Total Fluorescence (CTF) was calculated for each image: (Integrated Density of the area containing the animals) – [(Area containing the animals) x (Mean fluorescence of background)]. For all the experiments the sample size was determined considering the estimated variability of similar experiments reported in literature and of previous experiments performed in the laboratory. Animal have been divided by simple randomisation, since all animals originate from one plate with thousands of animals that are isogenic and clonal siblings from self-fertilizing homozygous hermaphrodites; no inclusion or exclusion criteria have been set and all animals scored have been included. To minimise potential confounders, we standardized treatment conditions by simultaneously treating animals with mock and SPIONs@SiO_2-PDA in the same 96-well plate. We performed a blind quantification when the *pgst-4::*GFP expression were evaluated by ImageJ software that provides unbiased data analysis. No blind analysis has been performed in other experiments considering the complex manipulation of animals required to perform them. No primary outcome measure has been used in this study. All animal experiments comply with ARRIVE guidelines and the U.K. Animals (Scientific Procedures) Act, 1986 and associated guidelines and with EU Directive 2010/63/EU for animal experiments.

Statistical analysis

For A549 toxicity screening, statistical analysis was performed using GraphPad Prism software with a regular two-way analysis of variance (ANOVA) followed by the Tukey multiple comparison test. All comparisons were considered significant when p was < 0.05. For the *in vivo* experiments in *C. elegans* non-parametric tests (One-way ANOVA Kruskal-Wallis test and Mann-Whitney *t*-test) were used for statistical analyses performed with GraphPad Prism and no relevant assumption has been tested. The effect size was calculated through dividing the difference between the two groups (the

mean of treatment group minus the mean of the control group) with the pooled standard deviation (Cohen's d formula with 95% Confidence Interval).

Results and discussion

Silica-coating and polydopamine functionalization

The effectiveness of the silica coating and the polydopamine surface functionalization was confirmed by XRD and FTIR. In figure 1b, the diffraction peaks at 2Θ = 18.80°, 30.01°, 35.60°, 43.51°, 53.78°, 57.46°, 62.97°, 71.41° and 74.54° can be assigned to (1 1 1), (2 2 0), (3 1 1), (4 0 0), (4 2 2), (5 1 1), (4 4 0), (6 2 0) and (5 5 3) planes by comparison with International Centre for Diffraction Data (ICDD no. 00-019-629), which correspond with an inverse spinel structure crystalline phase of magnetite [39]. In addition, we observed a broad band located between 15°-30° (blue pattern), representing the distinguishing feature of the amorphous nature of silica shells [40]. In figure 1c, SPIONs@SiO_2-PDA (blue pattern) and SPIONs@OA (black pattern) FTIR spectra showed similar bands around 580 cm^{-1}, attributed to the stretching vibration mode associated with the metal-oxygen Fe – O bonds in the crystalline lattice of Fe_3O_4 [41]. For SPIONs@OA, 2915, 2843, 1513, and 1409 cm^{-1} bands corresponded to stretching vibrations of CH_2 (asymmetric and symmetric) and the stretching modes (asymmetric COO^-, symmetric COO^-) of the oleic acid [41]. On the other hand, in SPIONs@SiO_2-PDA spectra, the silica-coating was further confirmed by the appearance of three peaks at 960, 440, and 810 cm^{-1}, corresponding to the stretching modes of Si-O-Si (asymmetric and symmetric) and the scissoring vibration of Si-O-Si, respectively. In addition, PDA functionalization was demonstrated by the presence of absorption bands at 3370, 2936, 2869, 1503, 1432, and 1340 cm^{-1}, associated with -NH stretching, -CH_2 (asymmetric and symmetric), -C=N stretching, -NH bending and -C-N-C stretching vibrations, respectively [42].

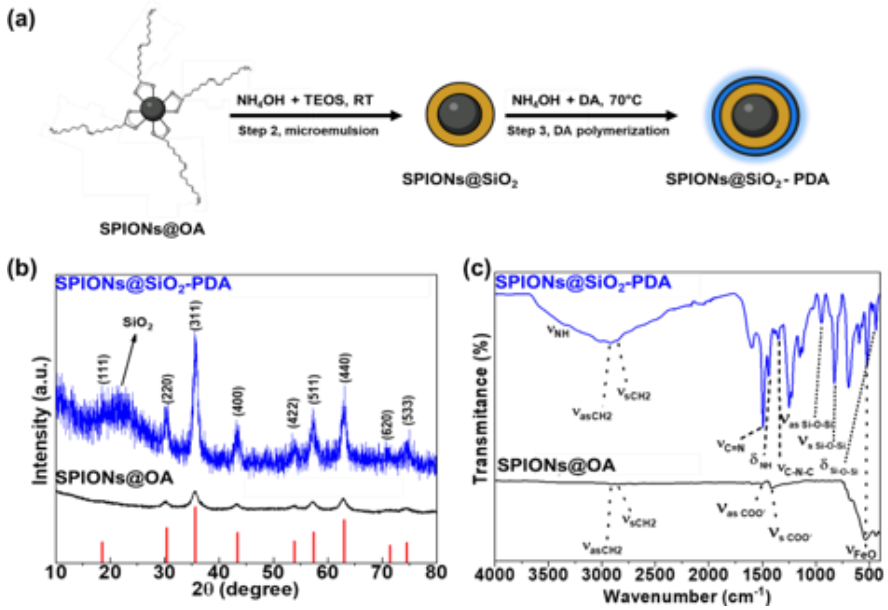

Figure 1. Demonstration of silica-coating and polydopamine functionalization. *(a) Scheme of the synthetic protocol used to obtain SPIONs@SiO_2-PDA; (b) X-ray diffraction (XRD) pattern of SPIONs@OA (black pattern) and SPIONs@SiO_2-PDA (blue pattern) compared to the XRD pattern of magnetite from the ICDD no. 00-019-629 database; (c) FTIR spectrum of the SPIONs@OA (black pattern) and SPIONs@SiO_2-PDA (blue pattern), with the characteristic bands as evidence.*

Morphological, optical, and magnetic characterization

SPIONs@SiO_2-PDA displayed spherical morphologies ranging in size around 20 nm (Fig. 2a-b) with magnetite cores (dark contrast) embedded inside a remarkable silica-coating, differently from what was observed with uncoated SPIONs@OA, which showed an irregular spherical shape with an average size of around 10nm (Fig. S2a-b. For further details, see supporting information). SPIONs@SiO_2-PDA presented a blue-colored fluorescent signal confirming the presence of fluorescent PDA on the surface, while no signals were observed SPIONs@OA (Fig. 2c-d).

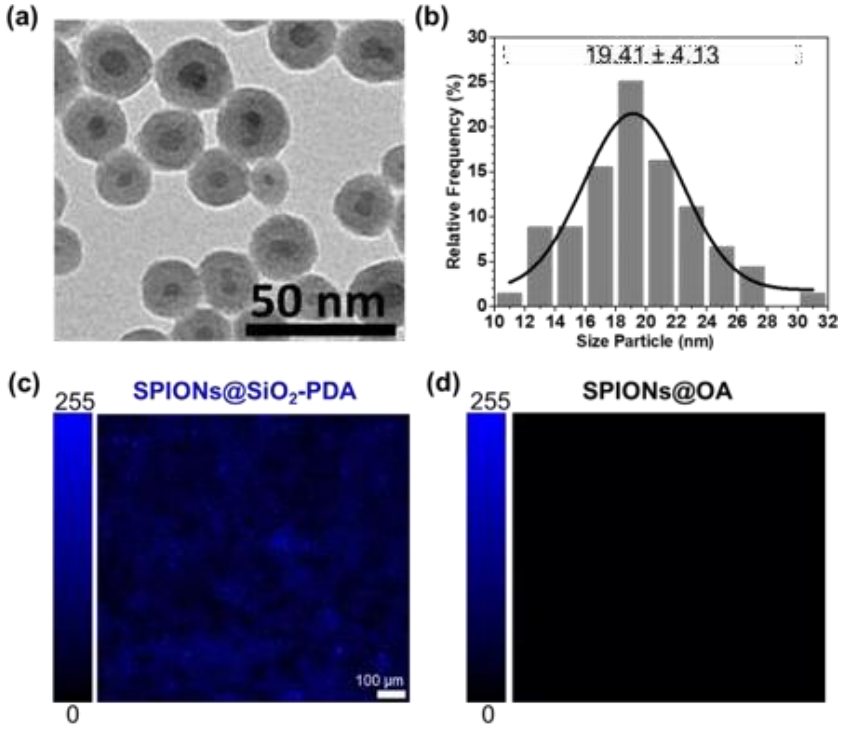

Figure 2. Morphological and optical properties of SPIONs@SiO$_2$-PDA. *(a) Representative TEM picture of SPIONs@SiO$_2$-PDA; (a) Size distribution of SPIONs@SiO$_2$-PDA performed with Image J software with N=400 nanoparticles; (c) Confocal fluorescence image of SPIONs@SiO$_2$-PDA and (d) SPIONs@OA.*

SPIONs@OA NPs presented negligible coercive fields (H_C = 3.5 Oe) and remanence (M_R = 0.6 emu/g_{Fe3O4}), corresponding to a superparamagnetic behavior at room temperature (Fig. S2c). In addition, the saturation magnetization of M_{sat}^{NP} = 63.7 emu/g_{Fe3O4} below the bulk magnetite value (92 emu/g_{Fe3O4}) was consistent with a surface inactive magnetic layer, a characteristic signature of the small size of the particles [43]. SPIONs@SiO$_2$-PDA magnetic properties were assessed under an applied magnetic field of 100 Oe in the field-cooled (FC) and zero-field-cooled (ZFC) regimes as a function of temperature (Fig. 3a). The ZFC curve reached the maximum at about 84 K, which corresponds to the blocking temperature (T_B) of the particles [44,45]. In contrast, at temperatures higher than 84K, they are in a superparamagnetic (SPM) regime since magnetization can randomly flip direction under the influence of temperature, and their time-averaged value is zero when there is no external field. In contrast, at temperatures higher than 84K, they are in a superparamagnetic (SPM) regime since

magnetization can randomly flip direction under the influence of temperature, and their time-averaged value is zero when there is no external field.

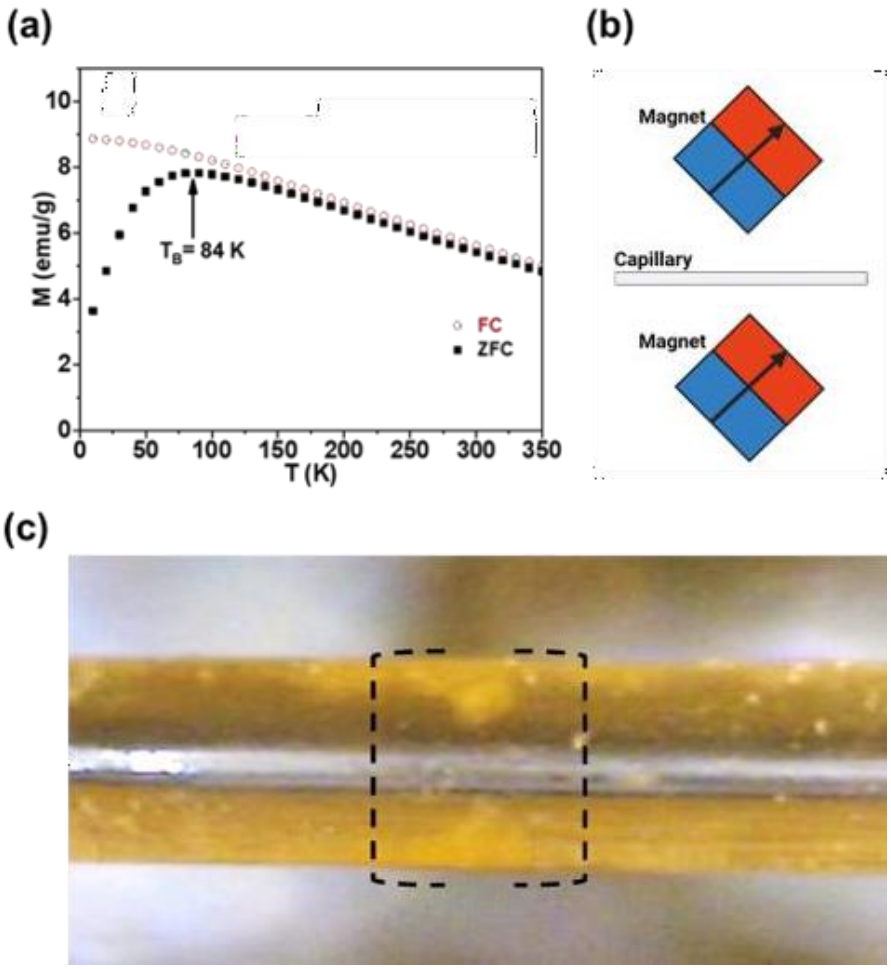

Figure 3. **SPIONs@SiO_2-PDA magnetic characterization and experimental realization of confinement by permanent magnets** *(a) ZFC and FC magnetization curves measured under an applied magnetic field of 100 Oe; (b) Configuration of the magnets in the experimental set-up; (c) SPION@SiO2@PDA are concentrated between the magnets in a clepsydra-shaped region spanning across the entire capillary section.*

The remarkable magnetic properties of SPIONs@SiO_2-PDA indicate their potential use as vehicles for drug delivery or hyperthermia treatments. Indeed, they can be effectively concentrated and confined in submillimeter-wide regions by a specially designed arrangement of commercial static magnets. It is composed of a couple of cubic 5x5x5 mm3 NdFeB permanent magnets with a remanence field of 1.3 T, spaced by 5 mm and oriented as shown in Fig. 3b. A transparent 500-µm wide quartz capillary, placed at the mid-point between the magnets, allows optical inspection of the

magnetic concentration. After a uniform solution of 1 mg/mL of SPION@SiO_2@PDA in de-ionized water (18 MΩ) was introduced in the capillary, the nanoparticles get concentrated (in ca.10 minutes) into a stable configuration between the magnets. It consists of two lobes at the capillary's walls united by a sharp vertex in the middle of the capillary (Fig. 3c). It is worth noticing here that, since the nanoplatforms can be easily collected by a magnetic field as experimentally demonstrated here, this can eliminate the cumbersome centrifugation procedures for collecting them.

Colloidal stability and physicochemical properties in cell culture media

Understanding NP's behavior in biological media is the first line of developing safe and effective nanomaterials. In complex biological solutions, NPs interact with the biomolecules presented in the media before getting in touch with cells. Fetal Bovine Serum (FBS) is a necessary supplement for cell culturing and is usually used to mirror a physiological environment in biological assays. FBS-derived constituents can affect NP physicochemical properties, influencing their biological performances [46]. For these reasons, we investigated SPIONs@SiO_2-PDA behavior in media with or without serum regarding colloidal stability and physicochemical properties (e.g., hydrodynamic diameter). Since cell culture media composition can vary according to the different cell types, DLS measurements were carried out in the two different cell culture media used for the biological *in vitro* assays, namely RPMI and DMEM:F12 with and without FBS. Data revealed that - once immersed in FBS-containing media (complete media) - SPIONs@SiO_2-PDA z-averaged hydrodynamic diameter D_z appeared 20% and 25% (cRPMI and cDMEM:F12, respectively) higher when compared to the size in water, likely due to the formation of an enhanced bio-corona around NPs (Table 1). On the other hand, SPIONs@SiO_2-PDA average diameters and size distributions remained unchanged in FBS-free media. It is worth noting that the measured size D_z = 105 nm was larger than the size determined by TEM measurements; these values are comparable if one converts from intensity averaged to number averaged size distribution [29]. DLS was also used to assess the stability of SPIONs@SiO_2-PDA in different media (S3). Interestingly, a slight fraction of aggregates below 1% was detected after 4h and 24h incubation in FBS-free media, indicating a marginal instability in these

buffers after long storage (Fig. S3a-c). At the same time, no changes in size distributions and stability were observed in complete media after 24h (S3b-d).

Solvent	Diameter z nm	PDI
Water	105 ± 5	0.27
RPMI	105 ± 5	0.27
DMEM:F12	105 ± 5	0.27
cRPMI	120 ± 10	0.19
cDMEM:F12	120 ± 10	0.19

Table 1. Physicochemical properties of SPIONs@SiO_2-PDA in culture media. *z-averaged hydrodynamic diameter D_z and the polydispersity indexes (PDI) in the different media; the same values were measured at each incubation time (4h and 24h).*

***In vitro* cytotoxicity and genotoxicity in the presence or not of serum**

One of the significant drawbacks contributing to the SPIONs' withdrawal from the market is the activation of unwanted immunological responses [47]. In most cases, immunotoxicity and toxicity can be driven by impurities and pyrogenic contamination derived from the synthetic process. SPIONs@SiO_2-PDA were analyzed for their endogenous content in LPS. For each sample, serial two-fold dilutions were tested until an endpoint was reached. The obtained values are depicted in Table 2. The endotoxin concentration was expressed as EU/mL for a correlation between the concentration of endotoxins in our materials and the LPS concentration used in the internal standard showing a small amount of endotoxins' contamination in the range of concentration used in the following biological assays.

Internal standard controls	NC (H_2O LAL)	0.0075 EU/mL	0.0125 EU/mL	0.03 EU/mL	0.06 EU/mL	PC 0.6 EU/mL
	-	-	-	+/-	+	+
SPIONs@ SiO_2-PDA	0.1 µg/mL	0.5 µg/mL	1 µg/mL	5 µg/mL	10 µg/mL	50 µg/mL
	-	-	-	+/-	+	+

Table 2. Assessment of endotoxin contamination of SPIONs@SiO_2-PDA dispersions at the concentrations used for the biological assays. *+ sign is used to define a positive endotoxin signal (i.e., gel cloth formation), while - or -/+ signs are used for samples where the endotoxin level is below the threshold level of detection (0,03 EU/mL). The negative control corresponds to pyrogen-free water and the positive control to the high concentration of endotoxins.*

In cell culture media (as well as in biological fluids), NPs come surrounded by proteins and other biomolecules, forming a protein corona (PC) through a reversible process that exchanges over time [48]. It has already been demonstrated that the PC derived from proteins in FBS-containing cell culture media can alter NP colloidal stability [49], impacting cellular interactions and leading to unexpected toxic effects or impaired intracellular internalization. Cellular uptake, tissue penetration, and toxicity of protein-coated SPIONs differ significantly from the pristine ones [7,50,51], and an overall analysis in different conditions is required. However, the toxicological effects of FBS-derived protein corona around the particles are unclear and differ from cell lines [49,52,53]. As expected, we observed that the *in vitro* toxic effects of SPIONs@SiO_2-PDA depended on the exposure media characteristics. LDH assay showed mild toxic effects (< 10%) in cells exposed for 4h in both complete and serum-free media (Fig. 4a). We observed a slight increase in the cytotoxicity levels when cells were treated with 10 µg/mL for 24h in serum-free media compared to the untreated cells (Fig. 4b). As shown in Fig. 4b, the highest concentration of SPION dispersions (50 µg/mL) in serum-free media caused a severe and significant increase in cytotoxicity, reaching ≥ 50% of cell death. No cytotoxicity was observed following 24h exposures in complete media. Analogously, Reczynska et al. [54] also obtained no cytotoxic effects in A549 cells exposed to 10µg/mL silica-coated SPIONs in media supplemented

with FBS. Results from the LDH assay were confirmed by the Alamar Blue assay, in which we analyzed the viability of metabolically active cells. Indeed, we did not observe any significant differences in cellular viability after 4h in both cell exposure conditions at each concentration, consistent with the low amount of LDH leakage (Fig. 4c). However, we saw a significant decrease in cell viability of approximately 90-fold in cells treated with 50 µg/mL in serum-free media for 24h compared to the relative control (Fig. 4d).

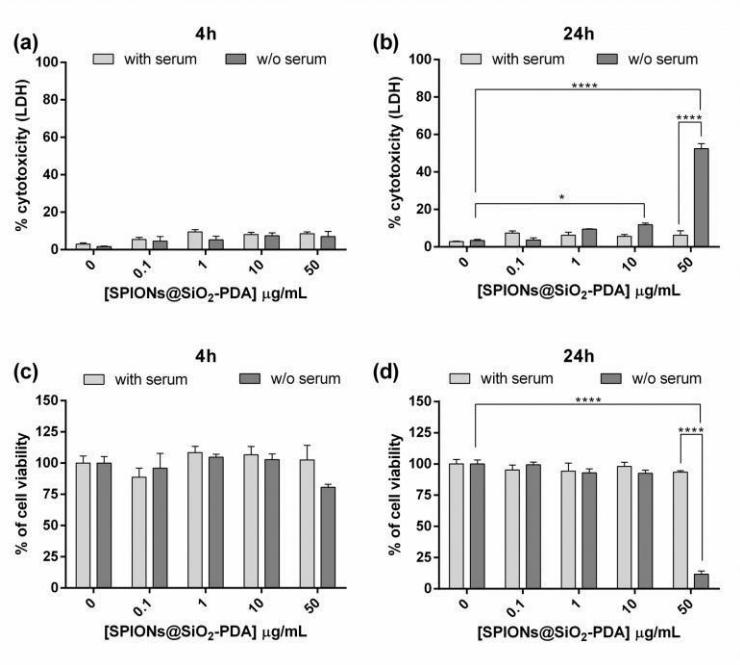

Figure 4. In vitro toxicity screening in A549 cells in the presence or not of serum.
*(a-b) Cytotoxicity measured by the LDH assay upon 4h (a) and 24h (b) exposures (n=3). (c-d) Cell viability measured by the Alamar Blue assay after 4h (c) and 24h (d) exposures (n=3); Legend: * = $p \leq 0.05$, **** = $p \leq 0.0001$.*

We also investigated clonogenicity, analyzing the ability of cells to survive and proliferate in colonies up to 10 days post-exposure. Though not statistically significant, we observed a slight decrease in the percentage of clonogenicity in A549 cells treated with all concentrations for 4h (Fig. 5a) and with the middle concentrations (1 µg/mL and 10 µg/mL) following 24h exposure in media with serum (Fig. 5b). Cells treated in serum-free media with the lowest (0.1 µg/mL) and middle concentrations showed a mild decrease in clonogenicity after 4h (Fig. 5a) and no significant increase after 24h with 0.1

µg/mL and 1 µg/ml treatments (Fig. 5b). Cells exposed to the highest concentration (50 µg/mL) for 4h in serum-free media presented a marked and significant decrease in clonogenicity of approximately 80 – 70-fold compared to the untreated and the cells treated with the same concentration but in media with serum (Fig. 5a). 24h exposures in serum-free media to the highest concentration caused a severe decrease in clonogenicity of approximately 80 – 60-fold, although not statistically relevant (Fig. 5b). The significant impairment in clonogenicity obtained with the highest concentration in the 4h and 24h serum-free exposures (Fig. 5a-b) might result from single and double DNA strand breaks. Genotoxicity analyses confirmed that SPIONs@SiO_2-PDA significantly increased strand breaks up to 4.9% to 8.9% when cells were treated for 4h (Fig. 5c) and 24h (Fig. 5d), respectively. Interestingly, the earlier time point (4h) showed significant damage also with the 10 µg/mL formulation compared to the untreated cells (4.4% DNA in tail) (Fig. 5c). On the other hand, we did not observe significant genotoxic effects when cells were treated in complete media at distinct time points and concentrations. In sum, both cytotoxic and genotoxic data confirmed the high biocompatibility of SPIONs@SiO_2-PDA once immersed in FBS-containing media at each time point and concentration.

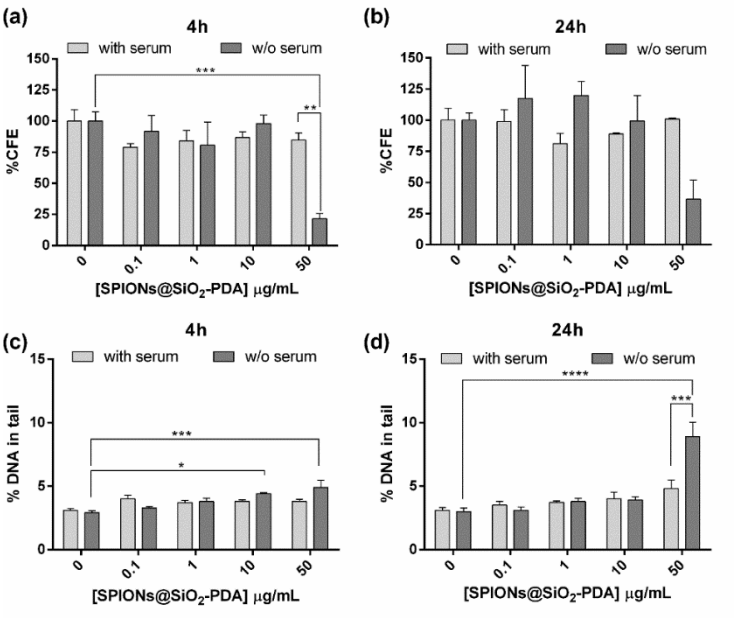

Figure 5. In vitro toxicity screening in A549 cells in the presence or not of serum.

*(a-b) Cytotoxicity measured by clonogenicity with the Colony Forming Efficiency assay (CFE) in cells treated for 4h (e) and 24h (f) (n=3). (c-d) DNA damage upon 4h treatments (g) and 24h (h) treatments. Legend: * = p ≤ 0.05, *** = p ≤ 0.001, **** = p ≤ 0.0001.*

In vitro and *ex vivo* immunotoxicity

Immunotoxicity was evaluated in THP-1 cell line with M0 macrophage-like phenotype in media supplemented with FBS. As for A549 cells, SPIONs@SiO_2-PDA did not affect cell viability after 24h and 48h hours at all the tested concentrations, but we observed a mild effect (<10%) following 72h exposures at the highest concentrations (Fig. 6a). Furthermore, to address immunotoxicity on human PBMC, we performed an *ex vivo* red blood cell hemolysis test (n=3) showing that SPIONs@SiO_2-PDA did not induce significant lysis of erythrocytes at the tested concentrations (Fig. 6b). Moreover, to study the potential allergenicity of the SPIONs, we applied an additional *ex vivo* assay using whole blood from healthy subjects (n= 4) on the attempt to detect possible immediate basophil activation. Our data showed that SPIONs@SiO_2-PDA do not display the ability to activate human basophil cells *per se*, showing a percentage of basophil activation similar to the negative control at the tested concentrations (Fig. 6c).

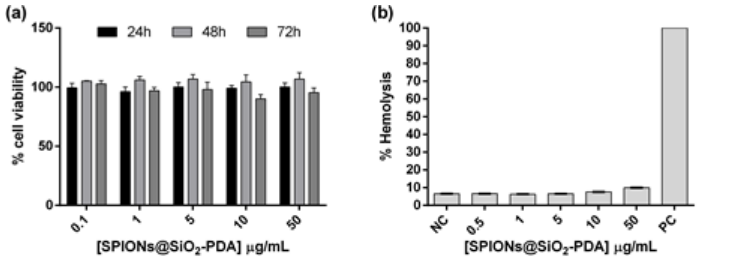

(c)

			SPIONs@SiO_2-PDA			
Subject	NC	PC	0.1 µg/mL	1 µg/mL	10 µg/mL	50 µg/mL
#1	0.3%	85.9%	0.2%	1%	1.3%	0
#2	0.4%	89.9%	0.4%	0.9%	1.1%	1.6%
#3	0.9%	44.2%	0.9%	1.5%	2.3%	1.6%
#4	1.5%	93.7%	0.6%	1.6%	0.6%	0.8%

Figure 6. In vitro and ex vivo immunotoxicity screening. *(a) Immunotoxicity measured by the MTS assay upon 24h, 48h and 72h (n=3); (b) Hemolytic potential in whole human blood sample; (c) Human basophil activation.*

***In vivo* toxicity**

The animal model *C. elegans* was used to evaluate SPIONs@SiO_2-PDA toxicity and bioactivity in the context of a whole living animal. Previous work demonstrated that exposure to iron NPs, uncoated or functionalized with different coating materials, can cause lethality, defects in growth and offspring, and defects in animal movement [55,56,57] We assessed the effects of the highest concentration (50 µg/mL) on animal fertility after chronic treatment, and, importantly, we did not observe any effect on animal brood size (Fig. 7a) nor on embryonic survival (Fig. 7b). However, at the same concentration, we observed a slight reduction in animal motility in water, a behavior called thrashing (Fig. 7c), similarly to what previously observed [56]. The biological significance calculated with Cohen's method corresponds to a d=0.68 (lower limit on d: 0.49, upper: 0.89), thus suggesting a medium effect size. Moreover, after treating animals with different concentrations of SPIONs@SiO_2-PDA (0.01, 0.1, 1, and 10 µg/mL), we confirmed a mild reduction of thrashing at all the concentrations used, except for 0.01 µg/mL, with a dose-dependent trend (Fig. 7c). Therefore, SPIONs@SiO_2-PDA are more compatible than other iron-NPs in respect to the fitness of the animal, but still cause a slight defect in locomotion. This interesting feature of SPIONs@SiO_2-PDA underlines the necessity of testing also locomotion as a more subtle and sensitive assay for assessing nanoparticles toxicity. Importantly this peculiar aspect deserves further investigation, but paves the way for further improvements to enhance SPIONs@SiO_2-PDA biocompatibility. In *C. elegans* alterations in dopamine content affect animal motility. In particular, a reduction in dopamine release causes a defect of thrashing [58], while excess of dopamine induces a SWimming Induced Paralysis (SWIP) [59]. Thus, we verified whether polydopamine in SPIONs@SiO_2-PDA could influence animal motility similarly to an excess of dopamine by performing the SWIP assay on treated animals and we did not observe any difference when comparing animals treated with mock or SPIONs@SiO_2-PDA (Fig. S4). These data strongly support for PDA not affecting animal motility *per se*.

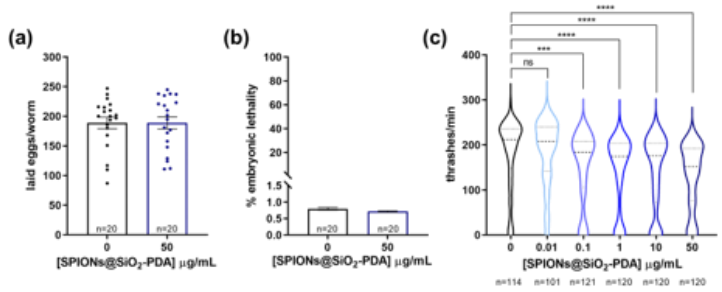

Figure 7. In vivo toxicity screening. (a) *Effect of SPIONs@SiO₂-PDA (SPIONs) on egg deposition. Each dot represents the number of laid eggs per P0 worm in the fertile period of the animal; n is the number of P0 parental animals analyzed.* ***(b)*** *Effect of SPIONs@SiO₂-PDA on embryonic survival. The percentage of unhatched eggs on the total number of laid eggs was calculated. Bars represent the mean, error bar is SEM. n is the number of P0 parental animals analyzed.* ***(c)*** *Effect of SPIONs@SiO₂-PDA on animal movement. Violin plots show the distribution of thrashes performed by the animals in a minute. Bold dashed line in the center correspond to the median while upper and lower dashed lines correspond to the quartiles. n is the number of total animals analyzed. Legend: ns corresponds to a p>0.9999; *** to a p<0.0005; **** p<0.0001 (One-way ANOVA Kruskal-Wallis test)..*

In vitro and *in vivo* oxidative stress evaluation

Oxidative stress represents one of the biggest concerns with the use of SPIONs. After being taken up by cells, SPIONs can be degraded inside lysosomal compartments, releasing free iron ions into the cytoplasm [7]. High levels of free iron ions increase the production of radical oxygen species (ROS), causing the oxidation of several biomolecules, including DNA and lipids. Silica coating has literature precedence in preventing particle intracellular degradation [11]. Still, the presence of a proteins around silica-coated SPIONs might have an active role in favoring the degradation of the silica-coating and, consequently, the iron ion leakage from the core [52]. Oxidative stress was assessed *in vitro* by measuring malondialdehyde (MDA) content in the culture media and *in vivo* in *C. elegans* by evaluating the expression levels of the homolog of the Glutathione S-transferase, *gst-4*, an essential gene involved in the detoxification process that promotes the oxidative stress resistance [60,61]. MDA is one of the final products of polyunsaturated fatty acids peroxidation in the cells, and it is often used as a marker of MDA as a marker of lipid peroxidation and oxidative stress. We observed no significant effects following 4h exposure both in media with and without serum (Fig. 8a). Twenty-four hours after exposure, MDA levels in cells treated in complete media were relatively lower than what we

observed after 4h exposures, indicating a time-dependent recovery process (Fig. 8b). On the other hand, we observed relevant increases of MDA levels after serum-free media treatments when cells were exposed to the higher concentration. In *C. elegans*, exposure to iron NPs can activate oxidative stress response and ROS accumulation [56]. To evaluate *gst-4* expression levels, we used a transgenic strain expressing GFP under the control of the *gst-4* promoter [38]. After treatments, we observed a significant increase in the expression of *pgst-4::*GFP fluorescence compared to animals treated with mock (Fig. 8c-d) and a very large size effect (Cohen's *d*=1.88, lower limit on *d*: 1.39, upper: 2.36), suggesting that chronic exposure to SPIONs@SiO_2-PDA can also induce an oxidative stress response *in vivo.*

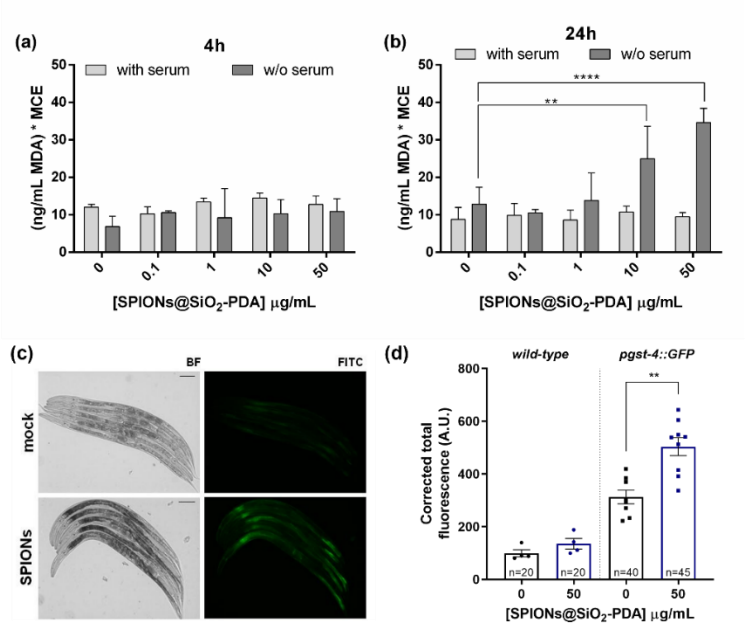

Figure 8. Activation of oxidative stress response in vitro and in vivo. *Malondialdehyde (MDA) levels [ng/ml] after 4h (a) and 24h (b) in A549 cells exposed to SPIONs@SiO_2-PDA measured in supernatant via LC-MS/MS. Data were normalized with the MCE derived from LDH values of the corresponding wells; (c) Representative images of pgst-4::GFP animals treated with mock (0)(upper panels) and SPIONs@SiO_2-PDA 50µg/mL (lower panels) and acquired with brightfield (BF) and epi-fluorescence (FITC) methods. The anterior part of the animal is on the left. Scale bar 75µm. (d) Quantification of the fluorescence in wild-type and pgst-4::GFP animals, after treatment with no SPIONs (0) or SPIONs@SiO_2-PDA 50µg/mL. Wild-type animals were also imaged to exclude any contribution of the intestinal autofluorescence to the analysis. Each dot represents the total fluorescence in the picture corrected for the background (CTF). Bars represent the mean, error bars are SEM. n is the total number of animals analyzed. Mann-Whitney t-test was used to establish the significance of treated pgst-4::GFP animals versus mock. Legend: ** p=0.0016.*

Intracellular uptake

Several studies reported that the FBS-derived proteins can also affect cellular uptake could lead to significant decreases in cellular uptake (Kiliç et al. 2015) [53]. Thus, the low cytotoxicity levels observed in our work might be related to a notable decrease in SPIONs@SiO_2-PDA cellular uptake when dispersed in complete media. The cellular uptake efficiency in the presence of serum proteins was markedly lower than for SPIONs@SiO_2-PDA incubated in serum-free conditions particularly following 24h exposure (Fig. 9). Notably, a certain degree of cytoskeleton disturbance can be observed after short term exposures in both tested conditions (Phalloidin staining, Fig. 9). Due to the role of the actin cytoskeleton in endocytosis, its disturbance might explain the minor uptake reduction observed following the shorter time-point exposures in both conditions. This observation is in line with the findings of Francia and co-authors on the complex role of cell receptors, protein corona formation, and actin disruption with inhibitors in the mechanisms used by cells to internalize silica NPs [63]. These aspects are of particular importance for the potential use of the developed SPIONs@SiO_2-PDA nanoplatform for nanomedicine purposes since *in vivo* NPs encounter much higher serum concentrations compared to *in vitro* scenario.

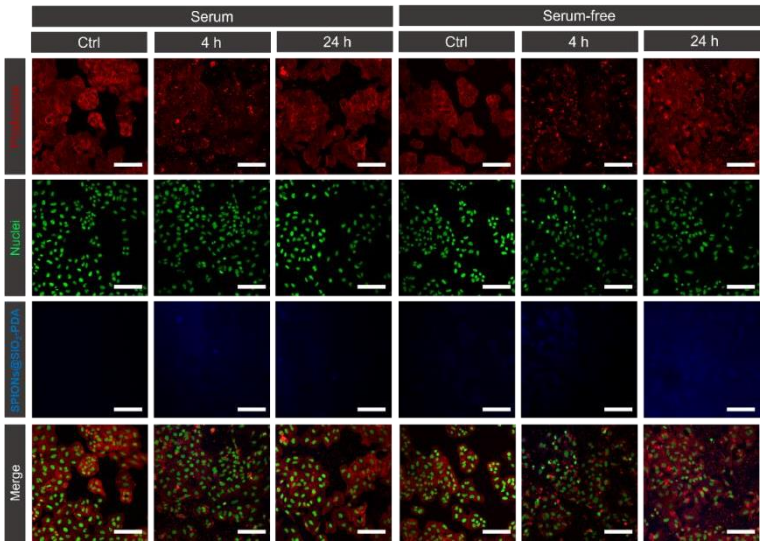

Figure 9. Intracellular uptake. *Confocal microscopy after 4h and 24h exposures in A549 cells with 50 µg/mL SPIONs@SiO_2-PDA in media with and without 5% serum. Actin cytoskeleton was stained with phalloidin, nuclei were stained with NucGreen Dead 488. Scale bar 100 µm.*

Conclusions

SPIONs' clinical application is hindered by several limitations related to safety and toxicity concerns. In the last years, the implementation of safe-by-design approaches to discover novel biocompatible shells contributed to minimize SPION toxicity. However, the flexibility in their synthetic route and the absence of gold standard methods often result in complex bio-nano interactions difficult to predict. As such, a comprehensive and systematic biological characterization – from *in vitro* to *in vivo* – is needed to assess toxicity risks and efficacies. In this study, we developed biocompatible silica-coated SPIONs functionalized with PDA with magnetic and fluorescent features. SPIONs@SiO_2-PDA were physicochemically characterized by complementary techniques, defining shape, morphology, and magnetic properties. SPIONs@SiO_2-PDA showed high stability in culture media supplemented with FBS, foreseeing their colloidal behavior in more complex true-to-life biological fluids. SPIONs@SiO_2-PDA proved to be biocompatible *in vitro* in FBS-containing media and *in vivo* in the invertebrate animal model *C.elegans*. Furthermore, the possibility of confining them in submillimeter-wide regions paves the way for their implementation for theranostic applications.

Supporting Information Available

The following files are available free of charge:

S1. Chemical details of the synthesis of silica-coated SPIONs functionalized with polydopamine.

S2. Morphological and magnetic characterization of SPIONs@OA precursor.

S3. Dynamic Light Scattering measurements.

S4. SWIP assay on animals treated with mock or SPIONs@SiO2-PDA.

ACKNOWLEDGEMENTS

This work was supported by the VES4US and the BOW projects funded by the European Union's Horizon 2020 research and innovation programme, under grant agreements No 801338 and 952183;

this work was also partially supported by the National Research Council (Seed DISBA-CNR Prize 2021)(E.D.S).

REFERENCES

1. Wu, K.; Su, D.; Liu, J.; Saha, R., Wang, J.P. Magnetic nanoparticles in nanomedicine: a review of recent advances. *Nanotechnology* **2019**, 30, p. 502003, DOI: 10.1088/1361-6528/ab4241.
2. Wáng, Y. X. J.; Idée, J. M. A comprehensive literatures update of clinical researches of superparamagnetic resonance iron oxide nanoparticles for magnetic resonance imaging. *Quantitative Imaging in Medicine and Surgery* **2017**, 7, pp. 88–122, DOI: 10.21037/qims.2017.02.09.
3. Piñeiro, Y.; Vargas, Z.; Rivas, J.; Lõpez-Quintela, M.A. Iron Oxide Based Nanoparticles for Magnetic Hyperthermia Strategies in Biological Applications. *European Journal of Inorganic Chemistry* **2015**, 27, pp. 4495–4509, 2015, DOI: 10.1002/ejic.201500598.
4. Wahajuddin, M.; Sumit, A. Superparamagnetic iron oxide nanoparticles: Magnetic nanoplatforms as drug carriers. *International Journal of Nanomedicine* **2012**, 7, pp. 3445–3471, DOI: 10.2147/IJN.S30320.
5. Schubert, J.; Chanana, M. Coating Matters: Review on Colloidal Stability of Nanoparticles with Biocompatible Coatings in Biological Media, Living Cells and Organisms. *Current Medicinal Chemistry* **2018**, 25, pp. 4553–4586, DOI:10.2174/0929867325666180601101859.
6. Vakili-Ghartavol, R.; Momtazi-Borojeni, A.A.; Vakili-Ghartavol, Z.; Aiyelabegan, H.T.; Jaafari, M. R.; Rezayat, S. M.; Bidgoli, S.A. Toxicity assessment of superparamagnetic iron oxide nanoparticles in different tissues. *Artificial cells, Nanomedicine and Biotechnology* **2020**, 48, pp. 443–451, DOI: 10.1080/21691401.2019.1709855.
7. Nelson, N.; Port, J.; Pandey, M. Use of Superparamagnetic Iron Oxide Nanoparticles (SPIONs) via Multiple Imaging Modalities and Modifications to Reduce Cytotoxicity: An Educational Review. *Journal of Nanotheranostics* **2020**, 1, pp. 105–135, DOI: 10.3390/jnt1010008.
8. Wei, H.; Hu, Y.; Wang, J.; Gao, X.; Qian, X.; Tang, M. Superparamagnetic iron oxide nanoparticles: Cytotoxicity, metabolism, and cellular behavior in biomedicine applications. *International Journal of Nanomedicine* **2021**, 16, pp. 6097–6113, 2021, DOI: 10.2147/IJN.S321984.
9. Mojica Pisciotti, M. L.; Lima, E.; Vasquez Mansilla, M.; Tognoli, V.E.; Troiani, H.E.; Pasa, A.A.; Creczynski-Pasa, T.B.; Silva, A.H.; Gurman, P.; Colombo, L.; Goya, G.F.; Lamagna, A.; Zysler, R.D. In vitro and in vivo experiments with iron oxide nanoparticles functionalized with DEXTRAN or polyethylene glycol for medical applications: Magnetic targeting. *Journal of Biomedical Materials Research - Part B Applied Biomaterials* **2014**, 102, pp. 860–868, DOI: 10.1002/jbm.b.33068.
10. Zavisova, V.; Koneracka, M.; Gabelova, A.; Svitkova, B.; Ursinyova, M.; Kubovcikova,M.; Antal, I.; Khmara, I.; Jurikova, A.; Molcan, M.; Ognjanović, M.; Antić, B.; Kopcansky, P. Effect of magnetic nanoparticles coating on cell proliferation and uptake. *Journal of Magnetism and Magnetic Material* **2018**, 472, pp. 66 - 73, DOI:10.1016/j.jmmm.2018.09.116.
11. Malvindi, M.A.; De Matteis, V.; Galeone,A.; Brunetti, V.; Anyfantis, G.C.; Athanassiou, A.; Cingolani, R.; Pompa, P.P. Toxicity assessment of silica coated iron oxide nanoparticles and biocompatibility improvement by surface engineering. *PLoS One* **2014**, 9, e85835, DOI:

10.1371/journal.pone.0085835.

12. Liu, X.; Cao, J.; Li, H.; Li, J.; Jin, Q.; Ren, K.; Ji, J. Mussel-Inspired Polydopamine: A Biocompatible and Ultrastable Coating for Nanoparticles in Vivo. *ACS Nano* **2013**, 7, pp. 9384–9395, DOI: 10.1021/nn404117j.

13. Jin, A.; Wang, Y.; Lin, K.; Jiang, L. Nanoparticles modified by polydopamine: Working as 'drug' carriers. *Bioactive Materials* **2020**, 5, pp. 522–541, DOI:10.1016/j.bioactmat.2020.04.003.

14. Siminzar, P.; Omidi, Y.; Golchin, A.; Aghanejad, A.; Barar, J. Targeted delivery of doxorubicin by magnetic mesoporous silica nanoparticles armed with mucin-1 aptamer. *Journal of Drug Targeting* **2020**, 28, pp. 92–101, DOI: 10.1080/1061186X.2019.1616745.

15. Singh, N.; Sallem, F.; Mirjolet, C.; Nury, T.; Sahoo, S.K.; Millot, N.; Kumar, R. Polydopamine modified superparamagnetic iron oxide nanoparticles as multifunctional nanocarrier for targeted prostate cancer treatment. *Nanomaterials (Basel)* **2019**, 9, p. 138, DOI: 10.3390/nano9020138.

16. Iacoviță, C.; Fizeșan, I.; Nitica, S.; Florea, A.; Barbu-Tudoran, L.; Dudric, R.; Pop, A.; Vedeanu, N.; Crisan, O.; Tetean, R.; Loghin, F.; Lucaciu, C.M., Silica Coating of Ferromagnetic Iron Oxide Magnetic Nanoparticles Significantly Enhances Their Hyperthermia Performances for Efficiently Inducing Cancer Cells Death In Vitro. *Pharmaceutics* **2021**, 13, p. 2026, DOI: 10.3390/pharmaceutics13122026.

17. Iqbal, M.Z.; Ma, X.; Chen, T.; Zhang, L.; Ren, W.; Xianga, L.; Wu, A. Silica-coated super-paramagnetic iron oxide nanoparticles (SPIONPs): a new type contrast agent of T1 magnetic resonance imaging (MRI). Journal of Materials Chemistry B 2015, 3, pp. 5172–5181, DOI: 10.1039/c5tb00300h.

18. Liao, N.; Wu, M.; Pan, F.; Lin, J.; Li, Z.; Zhang, D.; Wang, Y.; Zheng, Y.; Peng, J.; Liu, X.; Liu, J. Poly (dopamine) coated superparamagnetic iron oxide nanocluster for noninvasive labeling, tracking, and targeted delivery of adipose tissue-derived stem cells. *Scientific Reports* **2016**, 6, pp. 1–13, DOI: 10.1038/srep18746.

19. Quignard, S.; d'Ischia, M.; Chen, Y.; Fattaccioli, J. Ultraviolet-Induced Fluorescence of Polydopamine-Coated Emulsion Droplets. *Chempluschem*, **2014**, 79, pp. 1254–1257, DOI: 10.1002/cplu.201402157.

20. Madhurakkat Perikamana, S.K.; Lee, J.; Lee, Y.B.; Shin, Y.M.; Lee, E. J.; Mikos, A.G.; Shin, H. Materials from Mussel-Inspired Chemistry for Cell and Tissue Engineering Applications. *Biomacromolecules*, **2015**, 16, pp. 2541–2555, DOI:10.1021/acs.biomac.5b00852.

21. Faria, M.; Björnmalm, M.; Thurecht, K.J.; Kent, S.J.; Parton, R.G.; Kavallaris, M.; Johnston, A.P.R.; Gooding, J.J.;Corrie, S.R.; Boyd, B.J.; Thordarson, P.; Whittaker, A.K.; Stevens, M.M.; Prestidge, C.A.; Porter, C.J.H.; Parak, W.J.; Davis, T.P.; Crampin, E.J.; Caruso, F. Minimum information reporting in bio–nano experimental literature. *Nature Nanotechnology* **2018**, 13, pp. 777–785, DOI: 10.1038/s41565-018-0246-4.

22. González-Gómez, M.A.; Belderbos, S.; Yañez-Vilar, S.M.; Piñeiro, Y.; Cleeren, F.; Bormans, G.; Deroose, C.M.; Gsell, W.; Himmelreich, U.; Rivas, J. Development of Superparamagnetic Nanoparticles Coated with Polyacrylic Acid and Aluminum Hydroxide as an Efficient Contrast Agent for Multimodal Imaging. *Nanomaterials* **2019**; 9, 1626. DOI: 10.3390/nano9111626.

23. Moldes-Diz, Y.; Gamallo, M.; Eibes, G.; Vargas-Osorio, Z.; Vazquez-Vazquez, C.; Feijoo, G.; Lema, J.M.; Moreira, M.T. Development of a Superparamagnetic Laccase Nanobiocatalyst for

the Enzymatic Biotransformation of Xenobiotics. *Journal of Environmental Engineering* **2018**, 144, p. 4018007, DOI: 10.1061/(ASCE)EE.1943-7870.0001333.

24. Schmitz, K.S.; Phillies, G. D. J. An Introduction to Dynamic Light Scattering by Macromolecules. *Acadameic Press* **1990**. DOI: 10.1016/C2009-0-29091-X.

25. Poon, C. Measuring the density and viscosity of culture media for optimized computational fluid dynamics analysis of in vitro devices. *Journal of Mechanical Behavior of Biomedical Materials* **2022**, 126, p. 105024, DOI: 10.1016/j.jmbbm.2021.105024.

26. Romancino, D.P.; Buffa, V.; Caruso, S.; Ferrara, I.; Raccosta, S.; Notaro, A.; Campos, Y.; Noto, R.; Martorana; V.; Cupane, A.; Giallongo, A.; d'Azzo, A.; Manno, M.; Bongiovanni, A. Palmitoylation is a post-translational modification of Alix regulating the membrane organization of exosome-like small extracellular vesicles. *Biochimica et Biophysica Acta (BBA) - General Subjects* **2018**, 1862, pp. 2879–2887, DOI: 10.1016/j.bbagen.2018.09.004.

27. Paterna, A.; Rao, E.; Adamo, G.; Raccosta, S.; Picciotto, S.; Romancino, D.; Noto, R.; Touzet, N.; Bongiovanni A.; Manno, M. Isolation of Extracellular Vesicles From Microalgae: A Renewable and Scalable Bioprocess. *Frontiers in Bioengineering and Biotechnology* **2022**, 10, p. 836747, DOI: 10.3389/fbioe.2022.836747.

28. Rausch, K.; Reuter, A.; Fischer, K.; Schmidt, M. Evaluation of Nanoparticle Aggregation in Human Blood Serum. *Biomacromolecules* **2010**, 11, pp. 2836–2839, DOI:10.1021/bm100971q.

29. Adamo, G.; Fierli, D.; Romancino, D. P.; Picciotto, S.; Barone, M.E.; Aranyos, A.; Božič, D.; Morsbach, S.; Raccosta, S.; Stanly, C.; Paganini, C.; Gai, M.; Cusimano, A.; Martorana, V.; Noto, R.; Carrotta, R.; Librizzi, F.; Randazzo, L.; Parkes, R.; Palmiero, U.C.; Rao, E.; Paterna, A.; Santonicola, P.; Iglič, A.; Corcuera, L.; Kisslinger, A.; Di Schiavi, E.; Liguori, G.L.; Landfester, K.; Kralj-Iglič, V.; Arosio, P.; Pocsfalvi, G.; Touzet, N.; Manno, M.; Bongiovanni, A. Nanoalgosomes: Introducing extracellular vesicles produced by microalgae. *Journal of Extracellular Vesicles* **2021**, 10, DOI: 10.1002/jev2.12081.

30. Schindelin, J.; Arganda-Carreras, I.; Frise, E.; Kaynig, V.; Longair, M.; Pietzsch, T.; Preibisch, S.; Rueden, C.; Saalfeld, S.; Schmid, B.; Tinevez, J.I.; White, D.J.; Hartenstein, V.; Eliceiri, K.; Tomancak, P.; Cardona, A. Fiji: an open-source platform for biological-image analysis. *Nature Methods* **2012**, 9, pp. 676–682, DOI: 10.1038/nmeth.2019.

31. Di Bucchianico, S.; Cappellini, F.; Le Bihanic, F.; Zhang, Y.; Dreij, K.; Karlsson, H.L. Genotoxicity of TiO2 nanoparticles assessed by mini-gel comet assay and micronucleus scoring with flow cytometry. *Mutagenesis* **2017**, 32, pp. 127–137, DOI: 10.1093/mutage/gew030.

32. Xin, C.; Padoan, S.; Binder, S.; Bauer, S.; Orasche, J.; Rus, C.M.; Mudan, A.; Huber, A.; Kuhn, E.; Oeder, S.; Lintelmann, J.; Adam, T.; Di Bucchianico, S.; Zimmermann, R. A comparative study of persistent DNA oxidation and chromosomal instability induced in vitro by oxidizers and reference airborne particles. *Mutation Research/Genetic Toxicology and Environmental Mutagenesis* **2022**, 874–875, p. 503446, DOI:10.1016/j.mrgentox.2022.503446.

33. Heinrich, P.; Diehl, U.; Förster, F.; Braunbeck, T. Improving the in vitro ethoxyresorufin-O-deethylase (EROD) assay with RTL-W1 by metabolic normalization and use of β-naphthoflavone as the reference substance. *Comparative Biochemistry and Physiology Part C: Toxicology & Pharmacology **2014***, 164, pp. 27–34, DOI: 10.1016/j.cbpc.2014.04.005.

34. Bonura, A.; Passantino, R.; Costa, M.A.; Montana, G.; Melis, M.; Bondì, M.L.; Butteroni, C.;

Barletta, B.; Corinti, S.; Di Felice, G.; Colombo, P. Characterization of a Par j 1/Par j 2 mutant hybrid with reduced allergenicity for immunotherapy of Parietaria allergy. *Clinical & Experimental Allergy* **2012**, 42, pp. 471–480, DOI: 10.1111/j.1365-2222.2011.03938.x.

35. Brenner, S. The genetics of Caenorhabditis elegans. *Genetics* **1974**, 77, pp. 71–94, DOI: 10.1093/genetics/77.1.71.

36. Picciotto, S.; Santonicola, P.; Paterna, A.; Rao, E.; Raccosta, S.; Romancino, D.P.; Noto, R.; Touzet, N.; Manno, M.; Di Schiavi, E.; Bongiovanni, A.; Adamo, G. Extracellular Vesicles From Microalgae: Uptake Studies in Human Cells and Caenorhabditis elegans. *Frontiers in Bioengineering and Biotechnology* **2022**, 10, DOI: 10.3389/fbioe.2022.830189.

37. Lanzo, A.; Safratowich, B.D.; Kudumala, S.R.; Gallotta, I.; Zampi, G.; Di Schiavi, E.; Carvelli, L. Silencing of Syntaxin 1A in the Dopaminergic Neurons Decreases the Activity of the Dopamine Transporter and Prevents Amphetamine-Induced Behaviors in C. elegans. *Frontiers in Physiology* **2018**, 9, DOI: 10.3389/fphys.2018.00576.

38. Link, C.D.; Johnson, C.J. Reporter Transgenes for Study of Oxidant Stress in Caenorhabditis elegans. *Methods in Enzymology* **2002**, 353, pp. 497-505, DOI: 10.1016/s0076-6879(02)53072-x.

39. Kolen'ko, Y.V.; Bañobre-López, M.; Rodríguez-Abreu, C.; Carbó-Argibay, E.; Deepak, F.L.; Petrovykh, D.Y.; Cerqueira, M.F.; Kamali, S.; Kovnir, K.; Shtansky, D.V.; Lebedev, O.I.; Rivas, J. High-Temperature Magnetism as a Probe for Structural and Compositional Uniformity in Ligand-Capped Magnetite Nanoparticles. *The Journal of Physical Chemistry C* **2014**, 118, pp. 28322–28329, DOI: 10.1021/jp5106949.

40. Chitra, K.; Annadurai, G. Fluorescent Silica Nanoparticles in the Detection and Control of the Growth of Pathogen. *Journal of Nanotechnology* **2013**, 2013, p. 509628, DOI: 10.1155/2013/509628.

41. Nalbandian, L.; Patrikiadou, E.; Zaspalis, V.; Patrikidou, A.; Hatzidaki, E.; Papandreou, C. Magnetic Nanoparticles in Medical Diagnostic Applications: Synthesis, Characterization and Proteins Conjugation. *Curruent Nanoscience* **2016**, 12, pp. 455-468, DOI: 10.2174/1573413712666151210230002.

42. Cheng, W.; Fan, F.; Zhang, Y.; Pei, Z.; Wang, W.; Pei, Y. A Facile Approach for Fabrication of Core-Shell Magnetic Molecularly Imprinted Nanospheres towards Hypericin. *Polymers* **2017**, 9, p. 135, DOI: 10.3390/polym9040135.

43. Sato, T.; Iijima, T.; Seki, M.; Inagaki, N. Magnetic properties of ultrafine ferrite particles. *Journal of Magnetism and Magnetic Materials* **1987**, 65, pp. 252–256, 1987, DOI: 10.1016/0304-8853(87)90044-8.

44. Liu, C.; Zou, B.; Rondinone, A.J.; Zhang, Z.J. Chemical Control of Superparamagnetic Properties of Magnesium and Cobalt Spinel Ferrite Nanoparticles through Atomic Level Magnetic Couplings. *Journal of the American Chemical Society* **2000**, 122, pp. 6263–6267, DOI: 10.1021/ja000784g.

45. Bruvera, I.J.; Mendoza Zélis, P.; Calatayud, M.P.; Goya, G.F.; Sánchez, F.H. Determination of the blocking temperature of magnetic nanoparticles: The good, the bad, and the ugly. *Journal of Applied Physics* **2015**, 118, p. 184304, DOI: 10.1063/1.4935484.

46. Moore, T.L.; Rodriguez-Lorenzo, L.; Hirsch, V.; Balog, S.; Urban, D.; Jud, C.; Rothen-Rutishauser, B.; Lattuada, Petri-Fink, A. Nanoparticle colloidal stability in cell culture media and impact on cellular interactions. *Chemical Society Reviews* **2015**, 44, pp. 6287–6305, DOI:

10.1039/C4CS00487F.

47. Patil, R.M.; Thorat, N.D.; Shete, P.B.; Bedge, P.A.; Gavde, S.; Joshi, M.G.; Tofail, S.A.M.; Bohara, R.A. Comprehensive cytotoxicity studies of superparamagnetic iron oxide nanoparticles. *Biochemistry and Biophysics Reports* **2018**, 13, pp. 63–72, DOI: 10.1016/j.bbrep.2017.12.002.

48. Auría-Soro, C.; Nesma, T.; Juanes-Velasco, P.; Landeira-Viñuela, A.; Fidalgo-Gomez, H.; Acebes-Fernandez, V.; Gongora, R.; Almendral Parra, M.J.; Manzano-Roman, R.; Fuentes, M. Interactions of nanoparticles and biosystems: Microenvironment of nanoparticles and biomolecules in nanomedicine. *Nanomaterials* **2019**, 9, p. 1365, DOI: 10.3390/nano9101365.

49. Mbeh, D.A.; Javanbakht, T.; Tabet, L.; Merhi, Y.; Maghni, K.; Sacher, E.; Yahia, L.H. Protein Corona Formation on Magnetite Nanoparticles: Effects of Culture Medium Composition, and Its Consequences on Superparamagnetic Nanoparticle Cytotoxicity. *Journal of Biomedical Nanotechnology* **2015**, 11, pp. 828–840, DOI: 10.1166/jbn.2015.2000.

50. Hill, A.; Payne, C.K. Impact of Serum Proteins on MRI Contrast Agents: Cellular Binding and T(2) relaxation. *RSC Advances* **2014**, 4, pp. 31735–31744, DOI: 10.1039/C4RA04246H.

51. Vogt, C.; Pernemalm, M.; Kohonen, P.; Laurent, S.; Hultenby, K.; Vahter, M.; Lehtiö, J.; Toprak, M.S.; Fadeel, B. Proteomics analysis reveals distinct corona composition on magnetic nanoparticles with different surface coatings: Implications for interactions with primary human macrophages. *PLoS One* **2015**, 10, p. e0129008 DOI: 10.1371/journal.pone.0129008.

52. Kiliç, G.; Costa, C.; Fernández-Bertólez, N.; Pásaro, E.; Teixeira, J.P.; Laffon, B.; Valdiglesias, V. In vitro toxicity evaluation of silica-coated iron oxide nanoparticles in human SHSY5Y neuronal cells. *Toxicology Research* **2016**, 5, pp. 235–247, DOI: 10.1039/c5tx00206k.

53. Balk, M.; Haus, T.; Band, J.; Unterweger, H.; Schreiber, E.; Friedrich, R.P.; Alexiou, C.; Gostian, A.O. Cellular spion uptake and toxicity in various head and neck cancer cell lines. *Nanomaterials (Basel)* **2021**, 11, pp. 1–19, DOI: 10.3390/nano11030726.

54. Reczyńska, K.; Marszałek, M.; Zarzycki, A.; Reczyński, W.; Kornaus, K.; Pamuła, E.; Chrzanowski, W. Superparamagnetic iron oxide nanoparticles modified with silica layers as potential agents for lung cancer treatment. *Nanomaterials (Basel)* **2020**, 10, p. 1076, DOI: 10.3390/nano10061076.

55. Fajardo, C.; Costa, G.; Nande, M.; Martín, C.; Martín, M.; Sánchez-Fortún, S. Heavy metals immobilization capability of two iron-based nanoparticles (nZVI and Fe3O4): Soil and freshwater bioassays to assess ecotoxicological impact. *Science of The Total Environment* **2019**, 656, pp. 421–432, DOI: 10.1016/j.scitotenv.2018.11.323.

56. Wu, Q.; Li, Y.; Tang,M.; Wang, D. Evaluation of Environmental Safety Concentrations of DMSA Coated Fe2O3-NPs Using Different Assay Systems in Nematode Caenorhabditis elegans. *PLoS One* **2012**, 7, p. e43729, DOI: 10.1371/journal.pone.0043729.

57. Gonzalez-Moragas, L.; Yu, S.-M.; Carenza, E.; Laromaine, A.; Roig, A. Protective Effects of Bovine Serum Albumin on Superparamagnetic Iron Oxide Nanoparticles Evaluated in the Nematode Caenorhabditis elegans. *ACS Biomaterials Science & Engineering* **2015**, 1, pp. 1129–1138, DOI: 10.1021/acsbiomaterials.5b00253.

58. Mocko, J.B.; Kern, A.; Moosmann, B.; Behl, C.; Hajieva, P. Phenothiazines interfere with dopaminergic neurodegeneration in Caenorhabditis elegans models of Parkinson's disease. *Neurobiology of Disease* **2010**, 40, pp. 120–129, DOI: 10.1016/j.nbd.2010.03.019.

59. McDonald, P.W.; Hardie, S.L.; Jessen, T.N.; Carvelli, L.; Matthies, D.S.; Blakely, R.D. Vigorous Motor Activity in Caenorhabditis elegans Requires Efficient Clearance of Dopamine Mediated by Synaptic Localization of the Dopamine Transporter DAT-1. *Journal of Neuroscience* **2007**, 27, pp. 14216-14227, DOI: 10.1523/JNEUROSCI.2992-07.2007.

60. Hu, Q.; D'Amora, D.R.; MacNeil, L.T.; Walhout, A.J.M.; Kubiseski, T.J. The Caenorhabditis elegans Oxidative Stress Response Requires the NHR-49 Transcription Factor. *G3 Genes|Genomes|Genetics* **2018**, 8, pp. 3857–3863, DOI: 10.1534/g3.118.200727.

62. Oliveira, R.P.; Abate, J.P.; Dilks, K.; Landis, J.; Ashraf, J.; Murphy, C.T.; Blackwell, T.K. Condition-adapted stress and longevity gene regulation by Caenorhabditis elegans SKN-1/Nrf. *Aging Cell* **2009**, 8, pp. 524–541, DOI: 10.1111/j.1474-9726.2009.00501.x.

63. Francia, V.; Yang, K.; Deville, S.; Reker-Smit, C.; Nelissen, I.; Salvati, A. Corona Composition Can Affect the Mechanisms Cells Use to Internalize Nanoparticles. *ACS Nano* **2019**, 13, pp. 11107–11121, DOI: 10.1021/acsnano.9b03824.

Table of contents graphic (TOC)